Influence of Nanoparticles and Magnetic Field on the Laminar Forced Convection in a Duct Containing an Elastic Fin

ABDERRAHIM MOKHEFI[1], EUGENIA ROSSI DI SCHIO[2], PAOLO VALDISERRI[2,*], CESARE BISERNI[2]
[1]Mechanics, Modeling and Experimentation Laboratory L2ME,
Faculty of Technology,
Bechar University,
B.P.417, 08000, Bechar,
ALGERIA

[2]Department of Industrial Engineering DIN,
Alma Mater Studiorum – University of Bologna,
Viale Risorgimento 2, 40136, Bologna,
ITALY

**Corresponding Author*

Abstract: - In the present paper, an investigation of the effect of a magnetic field and nanoparticles suspended in pure water on the forced flow in a duct containing an elastic rectangular fin is performed. The nanofluid, i.e., CuO nanoparticles suspended in water, flow in the duct with an inlet fully developed velocity profile and a cold temperature. The lower boundary of the duct is kept at a hot temperature, while the upper boundary is adiabatic. According to the ALE formulation, numerical simulations of the laminar flow are carried out, by employing the software package Comsol Multiphysics, to solve the governing equation system: mass, momentum, energy, and deformation. The behavior of the Nusselt number, of the temperature and velocity fields as well as of the stress profiles are presented and interpreted. As a result, the addition of CuO nanoparticles to pure water improves the local and global heat transfer rate by up to 21.33% compared to pure water. On the other hand, it causes an additional deformation of the elastic fin as well as the increase of the stress due to the presence of the nanoparticles, leading to an increase of its maximum displacement of 34.58% compared to the case of pure water flow. Moreover, the enhancement of the flexibility of the fin (and thus its deformation) leads to a relative reduction in terms of convective heat transfer rate, especially downstream of the fin.

Key-Words: - nanofluid, elastic fin, nanoparticles, magnetic field, laminar flow, heat transfer.

Received: June 12, 2022. Revised: May 12, 2023. Accepted: June 21, 2022. Published: July 28, 2023.

1 Introduction

Elastic wall effects make the fluid dynamic problem very hard to treat theoretically; indeed, computational simulations for such configurations are necessary, [1]. This is even harder when nanoparticles are suspended in the base fluid, i.e. a nanofluid is employed, [2], [3], and when magnetohydrodynamic effects are investigated as well, [4].

Due to the importance of the flow around the fins or elastomeric structures and their sensibility especially in the industrial field, several previous works have been carried out in the literature. In, [5], the authors studied numerically the problem of unsteady natural convection inside an inclined square cavity equipped with a flexible impermeable membrane. They showed that in the case of a low Rayleigh number, the membrane shape is a function of the imposed body force. In, [6], the authors presented a theatrical study based on the numerical formulation of a fluid-structure interaction represented by an oscillating elastic fin attached to a hot vertical wall of a square cavity. They demonstrated that the increase of the oscillating fin amplitude can significantly enhance the Nusselt number. In, [7], the authors addressed the flow and heat transfer of a power-law non-Newtonian fluid in a cavity. The Arbitrary Lagrangian-Eulerian (ALE) along the moving mesh method is employed to model the deflection of the structure inside the fluid

domain. They showed that moving from pseudoplastic effects to Newtonian and dilatant effects increases the internal stresses in the fin. In, [8], the authors in their paper investigated the unsteady mixed convection in a cavity-channel assembly resulting from the interaction between fluid flow and a deformable (elastic) wall in the presence of a discrete heat source. They found that the presence of elastic walls enhances heat transfer efficiency compared to standard walls. In, [9], the authors reported techniques destined for the modelization of fluid-structure interactions using Comsol Multiphysics software. They illustrated the step followed to study the flow in a continuously deforming geometry based on the Arbitrary Lagrangian-Eulerian (ALE) technique and corresponding deformation, and displacement analysis.

In the case of general fluid flow in channels, several studies have been conducted in the literature based on computational fluid dynamics in the presence of different complex geometric shapes and different types of fluids including nanofluid. Indeed, the geometry of channels with an enclosed cavity has been investigated in, [10], [11], with reference to Couette flow, underlining the effects of thermophoresis and Brownian diffusion. In particular, in, [11], MHD effects are considered as well. In both papers, Buongiorno's model is employed, [12], [13].

The forced convection of nanofluids in the presence of MHD effects has been investigated in the literature with reference to lid-driven cavities or channels including an embedded cavity, [12], [14], [15]. In, [15], the roles of the dimensionless parameters are investigated showing that Lorentz force causes convection heat transfer to decrease.
Concerning the coupling of nanofluid convection with elastic walls/fins, attention has been paid especially to mixed convection, [16]; concerning forced convection, recently the arbitrary Lagrangian–Eulerian (ALE) technique has been used to numerically determine the interactions and movements of the nanofluid and fins, [17]. The investigated geometry was a rectangular enclosure, with two fins. As a result, the authors highlighted an increase in the heat transfer rate due to the oscillation of the fins. However, as far as the authors are concerned the simultaneous presence of elastic fins and MHD effects has not been investigated yet, with reference to channels with abruptly enlarged sections.

In the present paper, a numerical analysis of MHD effects on the forced convection of a CuO-water nanofluid is presented. In the literature, in, [18], it has been demonstrated this approach treats the structure in a fully Lagrangian way and uses an associated arbitrary Lagrangian-Eulerian (ALE) formulation for the fluid. Such a strategy has many advantages well detailed by Sotiropoulos and Yang. The fluid-solid interaction approach is employed to model the presence of an elastic fin. The geometry under investigation is a channel that displays an enclosure; the nanofluid enters the channel with a fully developed velocity profile and after a short entrance region a variation of the cross-section occurs, due to the presence of a cavity, and the fluid encounters an elastic fin. The effect of thermal boundary conditions is investigated as well.

2 Problem Formulation

2.1 Geometry Description

Let us investigate the effect of a vertical elastic fin inserted in a channel. The geometry under investigation is sketched in Fig. 1. We assume that after a short inlet region, with height H, where the nanofluid (water-CuO) has a fully developed parabolic profile velocity, the channel displays an increased height $2H$. Namely, a cavity or forward step occurs with a hot bottom boundary. Shortly after this increased height, a vertical elastic fin with height H is placed, acting as an activator of the turbulence in the nanofluid. Finally, traditional outlet conditions are prescribed at the end of the considered channel.

The thermophysical properties of the CuO nanoparticles and the base fluid are shown in Table 1.

Table 1. Thermophysical proprieties.

Properties	Water (f)	CuO (p)
Density [kg/m^3]	997.1	6500.0
Thermal capacity [J/(kg K)]	4179	540.00
Thermal conductivity [W/(m K)]	0.613	18.000
Dynamic viscosity [kg/(m s)]	0.001	--
Electrical conductivity [S/K]	0.05	2.7×10^{-8}

2.2 Governing Equations

2.2.1 Dimensional Governing Equations

The laminar flow inside the channel is governed by mass, momentum, and energy balances. In addition, the stress and the displacement of the elastic

structure (fin) are governed by the structure equation. In a Cartesian referential the local balance equations of the nanofluid part are given by local mass, momentum, and energy equations:

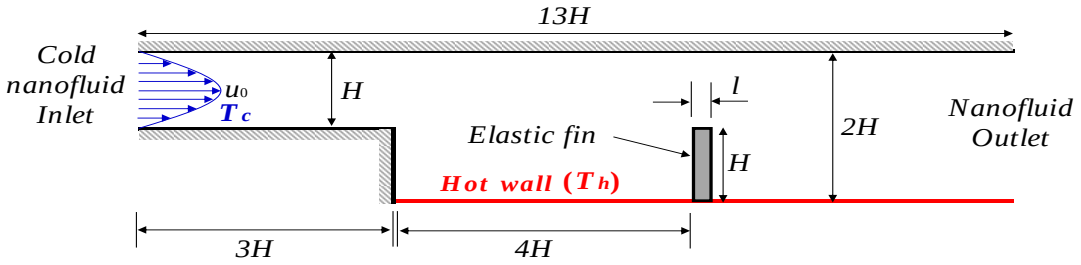

Fig. 1: Geometry of the channel containing an elastic fin

$$\frac{\partial u}{\partial x} + \frac{\partial v}{\partial y} = 0 \tag{1}$$

$$\rho_{nf}\left(\frac{\partial u}{\partial t} + (u - u_s)\frac{\partial u}{\partial x} + (v - v_s)\frac{\partial u}{\partial y}\right) = -\frac{\partial p}{\partial x} + \mu_{nf}\left(\frac{\partial^2 u}{\partial x^2} + \frac{\partial^2 u}{\partial y^2}\right) + \sigma_{nf} B_0^2 (v \cos\gamma \sin\gamma - u \sin\gamma) \tag{2}$$

$$\rho_{nf}\left(\frac{\partial v}{\partial t} + (u - u_s)\frac{\partial v}{\partial x} + (v - v_s)\frac{\partial v}{\partial y}\right) = -\frac{\partial p}{\partial y} + \mu_{nf}\left(\frac{\partial^2 v}{\partial x^2} + \frac{\partial^2 v}{\partial y^2}\right) + \sigma_{nf} B_0^2 (u \cos\gamma \sin\gamma - v \cos\gamma)) \tag{3}$$

$$\frac{\partial T}{\partial t} + (u - u_s)\frac{\partial T}{\partial x} + (v - v_s)\frac{\partial T}{\partial y} = \alpha_{nf}\left(\frac{\partial^2 T}{\partial x^2} + \frac{\partial^2 T}{\partial y^2}\right) \tag{4}$$

In the solid (elastic fin) part, the governing equations are written as:

$$\rho_s \frac{\partial^2 w}{\partial t^2} + P\sigma_s = 0 \tag{5}$$

$$\frac{\partial T_s}{\partial t} = \alpha_s\left(\frac{\partial^2 T_s}{\partial x^2} + \frac{\partial^2 T_s}{\partial y^2}\right) \tag{6}$$

where w and σ denote the local velocity and solid stress tensor, respectively. A detailed description of the fluid-solid interaction model, including the presence of a nanofluid and of the Lorentz force can be found in, [19].

2.2.2 Dimensionless Governing Equations

In order to make the studied problem more general, the following set of dimensionless variables has been introduced:

$$\begin{aligned} &X = \frac{x}{H},\ Y = \frac{y}{H},\ W = \frac{w}{H} \\ &U = \frac{u}{u_0},\ V = \frac{v}{u_0},\ P = \frac{p}{\rho_{nf} u_0^2}, \\ &\theta = \frac{T - T_c}{T_h - T_c}, \theta_s = \frac{T_s - T_c}{T_h - T_c}, \\ &t = \frac{u_0 t}{H}, \bar{\sigma} = \frac{\sigma}{E} \end{aligned} \tag{7}$$

After substituting Eq. (7) into Eqs. (1)-(6), they are rewritten as follows.
In the nanofluid part:

$$\frac{\partial U}{\partial X} + \frac{\partial V}{\partial Y} = 0 \tag{8}$$

$$\frac{\partial U}{\partial t} + U\frac{\partial U}{\partial X} + V\frac{\partial U}{\partial Y} = -\frac{\partial P}{\partial X} + \frac{\mu_{nf}}{\mu_f}\frac{1}{\mathrm{Re}}\left(\frac{\partial^2 U}{\partial X^2} + \frac{\partial^2 U}{\partial Y^2}\right) + \frac{\rho_f}{\rho_{nf}}\frac{\sigma_{nf}}{\sigma_f}\frac{\mathrm{Ha}^2}{\mathrm{Re}}(V \cos\gamma \sin\gamma - U \sin^2\gamma) \tag{9}$$

$$\frac{\partial V}{\partial t} + U\frac{\partial V}{\partial X} + V\frac{\partial V}{\partial Y} = -\frac{\partial P}{\partial X} + \frac{u_{nf}}{u_f}\frac{1}{\mathrm{Re}}\left(\frac{\partial^2 V}{\partial X^2} + \frac{\partial^2 V}{\partial Y^2}\right) + \frac{r_f}{r_{nf}}\frac{s_{nf}}{s_f}\frac{\mathrm{Ha}^2}{\mathrm{Re}}(U\cos\gamma\sin\gamma - V\cos^2\gamma) \quad (10)$$

$$\frac{\partial q}{\partial t} + U\frac{\partial q}{\partial X} + V\frac{\partial q}{\partial Y} = \frac{a_{nf}}{a_f}\frac{1}{\mathrm{Re}\,\mathrm{Pr}}\left(\frac{\partial^2 q}{\partial X^2} + \frac{\partial^2 q}{\partial Y^2}\right) \quad (11)$$

In the solid fin:

$$\frac{\mathrm{Ca}}{r_r}\frac{\partial^2 W}{\partial t^2} + \mathrm{P}\bar{s} = 0 \quad (12)$$

$$\frac{\partial q_s}{\partial t} = \frac{a_r}{\mathrm{Re}.\mathrm{Pr}}\left(\frac{\partial^2 q_s}{\partial X^2} + \frac{\partial^2 q_s}{\partial Y^2}\right) \quad (13)$$

The dimensionless stream function ψ is introduced to represent the streamlines of fluid along which this function is constant. It is calculated as

$$V = -\frac{\partial y}{\partial V} \text{ and } U = \frac{\partial y}{\partial Y} \quad (14)$$

The stream function is determined by solving the Poisson equation obtained by deriving the two members of Eq. (14) respectively with respect to X and Y, namely:

$$\frac{\partial^2 y}{\partial X^2} + \frac{\partial^2 y}{\partial Y^2} = -\frac{\partial V}{\partial X} + \frac{\partial U}{\partial Y} \quad (15)$$

The value of the stream function ψ, on the upper wall of the channel, is zero.

In Eqs. (7)-(13), the following dimensionless parameters have been introduced: the Reynolds number Re, the Hartmann number Ha, the Prandtl number Pr, and the Cauchy number Ca:

$$\mathrm{Re} = \frac{u_0 H}{J_f}, \mathrm{Ha} = B_0 H\sqrt{\frac{s_f}{r_f J_f}}, \mathrm{Pr} = \frac{J_f}{a_f}, \mathrm{Ca} = \frac{r_f u_0^2}{E} \quad (16)$$

Moreover, the reference parameters appearing in the set of the dimensionless governing equation for the fin are the relative density, the relative density, and the relative thermal diffusivity, given by:

$$r_r = \frac{r_s}{r_f} \text{ and } a_r = \frac{a_s}{a_f} \quad (17)$$

The density, electrical conductivity, thermal capacity, thermal conductivity coefficient, and dynamic viscosity of the CuO-water nanofluid are respectively calculated under the following relationships using the properties of the nanoparticles and the base fluid:

$$r_{nf} = (1-\varphi)r_f + \varphi r_p \quad (18)$$

$$s_{nf} = (1-\varphi)s_f + \varphi s_p \quad (19)$$

$$(rc_p)_{nf} = (1-\varphi)(rc_p)_f + \varphi(rc_p)_p \quad (20)$$

$$a_{nf} = k_{nf}/(rc_p)_{nf} \quad (21)$$

$$m_{nf} = m_f(1-\varphi)^{-2.5} \quad (22)$$

$$\frac{k_{nf}}{k_f} = \frac{k_p + 2k_f - 2\varphi(k_f - k_p)}{k_p + 2k_f + \varphi(k_f - k_p)} \quad (23)$$

2.3 Initial and Boundary Conditions

The governing differential equations system is solved together with the following initial-boundary conditions.

- At the initial time $\tau = 0$:

In the nanofluid domain

$$U = V = 0 \text{ and } q = 0 \quad (24)$$

In the fin domain

$$q_s = 0 \text{ and } W = 0 \quad (25)$$

- At the time $\tau \geq 0$:

Inlet: $U = -4Y^2 + 4Y$ and $q = 0$ (26)

Lower wall: $U = V = 0$, $q = 1$ and $W = 0$. (27)

Outlet: $\frac{\partial U}{\partial X} = \frac{\partial V}{\partial X} = \frac{\partial q}{\partial X} = 0$ (28)

Solid-fluid interface: $\frac{\partial W}{\partial X} = u$, $\frac{\partial W}{\partial Y} = v$ and $\frac{\partial q}{\partial N} = k_r\frac{\partial q_s}{\partial N}$ (29)

Other walls: $U = V = 0$, and $\frac{\partial q}{\partial N} = 0$ (30)

2.4 Heat Transfer Rate

Concerning nanofluid studies, the local Nusselt number is numerically calculated at any position of the duct as:

$$\mathrm{Nu} = -\frac{k_{nf}}{k_f}\frac{\partial q}{\partial Y} \quad (31)$$

Moreover, an averaged Nusselt number is defined as the average of the local Nusselt number along the hot wall:

$$\overline{\mathrm{Nu}} = \frac{1}{10H}\int_{\text{hot wall}} \mathrm{Nu}\,dX \quad (32)$$

3 Numerical Method

A Galerkin finite element method is used to solve the set of nonlinear governing equations, employing ALE techniques. For this purpose, Comsol Multiphysics software has been implemented to simulate the studied fluid-structure interaction phenomenon. Non-uniform triangular elements are used to build the mesh of the nanofluid domain. The fully coupled approach is used to couple the thermal, momentum, structure, and displacement of the mesh. The Computational domain mesh is presented in Figure 2.

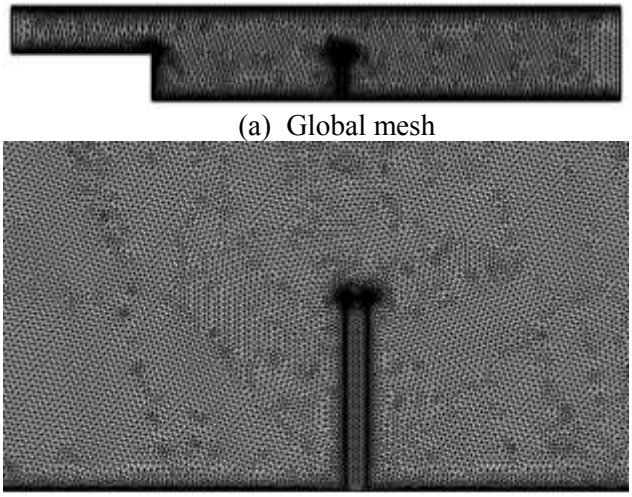

(a) Global mesh

(b) Mesh of the fin area

Fig. 2: Computational domain mesh.

3.1 Mesh Check and Numerical Validation

In order to obtain precise numerical results from the simulation, a study of mesh independence has been performed. The objective is to choose a suitable number of elements beyond which the results of the different global quantities remain unchanged depending on the mesh size. For this goal, we chose the average Nusselt number on the hot wall and the maximal displacement of the elastic fin as controlled characteristics, determined for different numbers of meshes as reported in Table 2.

Table 2. Evolution of the average Nusselt number and the maximal displacement as a function of mesh

Mesh	M1	M2	M3	M4
Elements	3215	5437	14866	23607
Nu	2.78383	2.60660	2.45259	2.45091
W_{max}	0.05904	0.05914	0.05940	0.05936

The mesh check has been performed in the case of Re = 100, Pr = 6.8, Ca = 10^{-4}, φ_0 = 0.04, and Ha = 0. It has been opted for a mesh corresponding to an element number equal to 14866 beyond which there was no change in terms of computational Nusselt number and maximal fin displacement results. In fact, a finer mesh leads to a variation of 7 x 10^{-4} % both in the Nusselt number and in the maximum displacement. In addition, in order to complete the calculation based on the number of iterations, the convergence criterion used includes the point at which the absolute difference between the old value and the new value of the dependent variable becomes less than 10^{-6}.

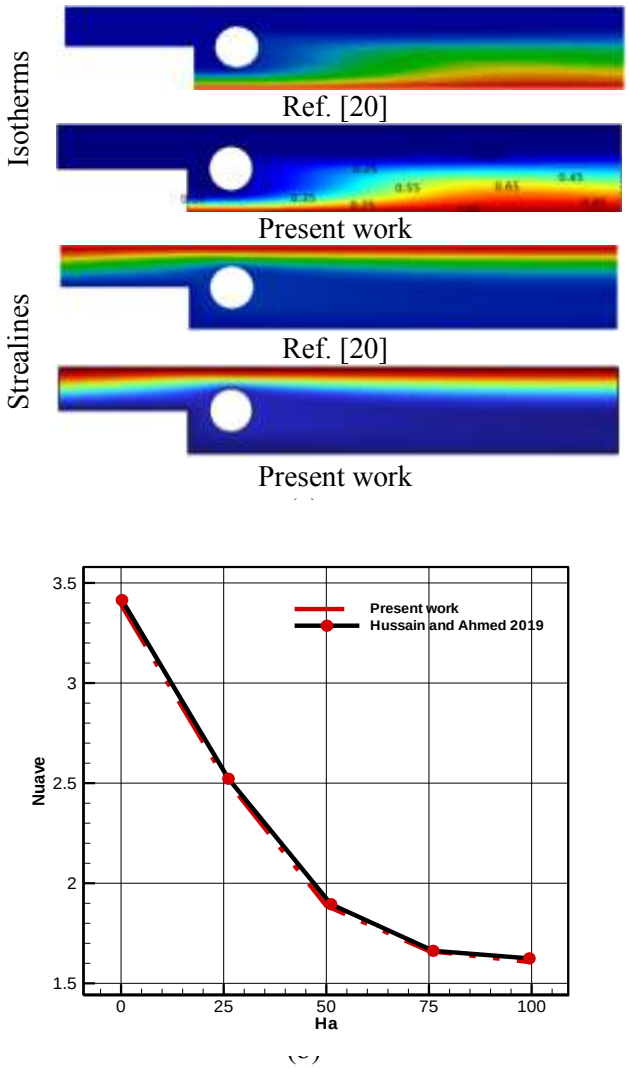

Fig. 3: Comparison of isotherms and streamlines (a) and of the average Nusselt number (b) with [20]

To evaluate the verification of the computational code, the numerical results of the present work have been compared with the numerical results of, [20]. In this reference, laminar forced convection of a nanofluid in the presence of a magnetic field has been studied inside an enlarged channel. The dimensionless stream function and temperature profiles obtained from the present work, as well as the average Nusselt number, have been compared with the results of the literature, [20], in

Figure 3, the comparison has been performed in the case of Re = 100, Pr = 6.2, Re = 100, $\gamma = 0°$, Ha = 100 and $\varphi = 0.05$. The agreement between the different results shown in Fig. 3 is excellent, thus validating the magnetohydrodynamic model of the present investigation.

Moreover, to solidify the validation of our work, we validated it also with previous work concerning fluid-structure interaction. Thus, we referred to the work of, [7], in which natural laminar convection was studied in the presence of an elastic fin. Ra = 10^5, Pr = 10, $E_t = 10^{10}$ and n = 1. The isotherms and streamlines are presented according to the chosen parameters, Figure 4. Moreover, the average Nusselt number for different Rayleigh numbers is shown in Table 3.

Figure 4 and Table 3 show that the results obtained from our code are in very good agreement with the results of the reference.

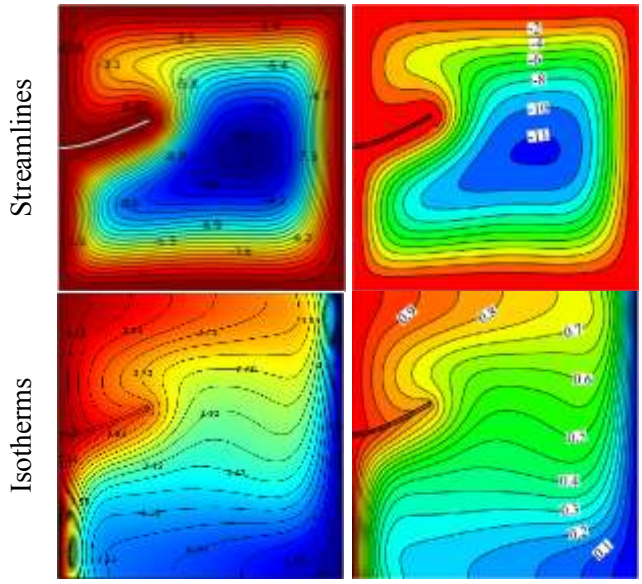

Fig. 4: Comparison of isotherms and streamlines with the reference, [7]

Table 3. Comparison of the Nusselt number from the present code with the reference, [7]

Ra	Shahabadi et al. (2021)	Present paper	% deviation
10^3	1.11405	1.20173	7,29
10^4	1.91530	1.84274	3,93
10^5	4.43836	4.40580	0,73

4 Results and Discussion

The results of the numerical simulation of the flow are presented in the form of temperature contours, flow streamlines as well as stress and displacement field of the elastic fin. Moreover, the heat transfer rate is analyzed through the local Nusselt number curves along the hot wall and through its average value for different parameters. The mechanical behavior of the elastic fin is highlighted by evaluating its maximum displacement. The results, and mainly the discussion, will be presented by evaluating separately, in dedicated subsections, the occurring effects, i.e. inertia, nanoparticle concentration, magnetic field, and elasticity. The control parameters are the Reynolds number, the volume fraction of CuO nanoparticles, the Hartmann number, and the Cauchy number. The reference thermo-physical properties of the elastic fin are fixed at: $\rho_r = C_{pr} = 1$ and $k_r = 100$.

4.1 Inertia Effect

The effect of inertia on the behavior of the nanofluid flowing in the extended pipe and on the mechanical behavior of the flexible fin is reflected by the influence of the initial velocity of the flow and is highlighted through the Reynolds number.

Figure 5 shows the temperature profile of the fluid and solid fin, the flow streamlines as well as the stress profile applied on the elastic fin for different Reynolds numbers. During the flow in the abruptly widened pipe equipped with an elastic fin, two vortices are developed. One is located downstream of the widening and the other downstream of the fin. These two vortex areas become larger and larger as the Reynolds number increases and the flow consequently becomes more intense. On the other hand, by analyzing the temperature contours of the nanofluid and the solid fin, it is observed that the thermal behavior is strongly dependent on the hydrodynamic behavior. Indeed, the thermal boundary layer decreases with the increase of the Reynolds number especially downstream of the fin. On the other hand, due to the conductive heat transfer mechanism at the solid fin, the isothermal lines refract horizontally when crossing the solid fin. Moreover, for all values of Reynolds number, the thermal boundary layer is of significant size in the vicinity of the fin and particularly at its immediate downstream, in the direction of the nanofluid flow. Due to the flexibility of the fin and its average elasticity (Ca = 10^{-4}), the nanofluid imposes on the walls of the fin a force resulting from viscous drag and pressure leading to a mechanical deformation by bending in the direction of flow. Indeed, under the applied load, all the points forming the structure except those of the embedding area (fin) tend to move in the direction of the nanofluid flow with an increasing intensity from the bottom to the top of the structure.

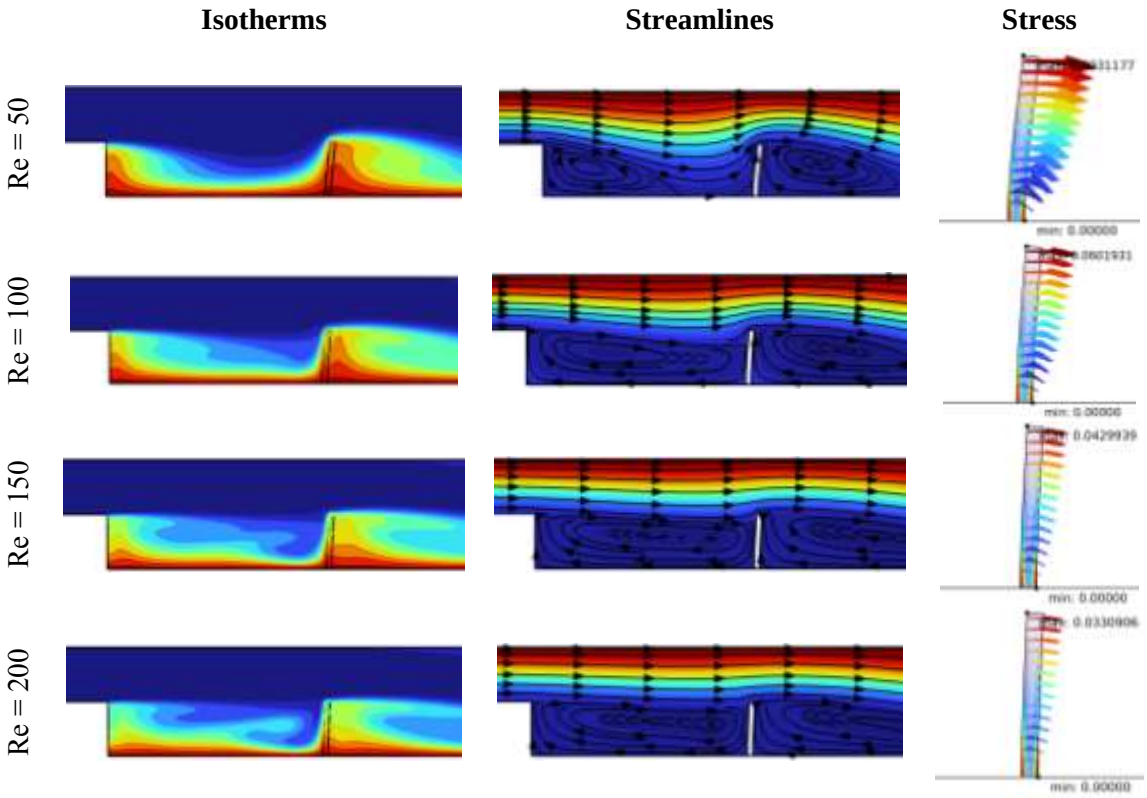

Fig. 5: Isotherms, streamlines, and stress for different values of Re

The stress applied by the nanofluid to the walls of the structure is more important at the lower corners of the structure (embedding zone of the embedding). With the increase of the Reynolds number, the maximum stress applied to the walls of the structure decreases so its displacement decreases under the effect of the inertia.

This is due to the increase of the flow intensity as well as the force applied due to the enlargement of the recirculation zone formed downstream of the structure which pushes the fin towards its primary stability state (reverse flow direction). Furthermore, the maximum displacement of the vane is at the upper left point of the structure. According to the stress profile analysis, as the Reynolds number increases, the maximum fin displacement decreases, as shown in Figure 6.

Figure 7 (a) presents the local Nusselt number along the hot wall of the pipe for different Reynolds numbers. Along this line and towards the elastic structure the rate of heat transfer increases and then decreases as one approaches the structure. This decrease in heat transfer becomes abrupt in the immediate vicinity of the structure as the Reynolds number increases toward the value of 200. Overall, along the line of measurement, the highest heat transfer rate depends on the large value of the Reynolds number. Since the Nusselt number is a thermal characteristic that identifies the convective heat transfer rate, the decrease in its value near the solid structure is due to the conductive heat transfer mechanism or the size of the hot thermal layer in this area on the one hand, and the thermal conductivity of the structure 100 times greater than that of the base fluid on the other.

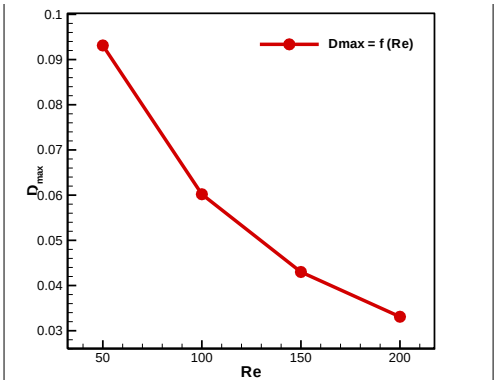

Fig. 6: Maximal fin displacement for various Reynolds numbers

Regarding the abruptness of the decrease of the heat transfer rate in the proximity of the structure corresponding to the important values of the Reynolds number, it is due to the intensification of the vortex flow upstream and downstream of the structure. Indeed, the increase of the velocity in the

vortex zones enhances the convective heat transfer and consequently, the influence of pure conduction is limited exactly to the interior of the structure. The overall heat transfer increases with increasing Reynolds number, as well evident in Figure 7 (b).

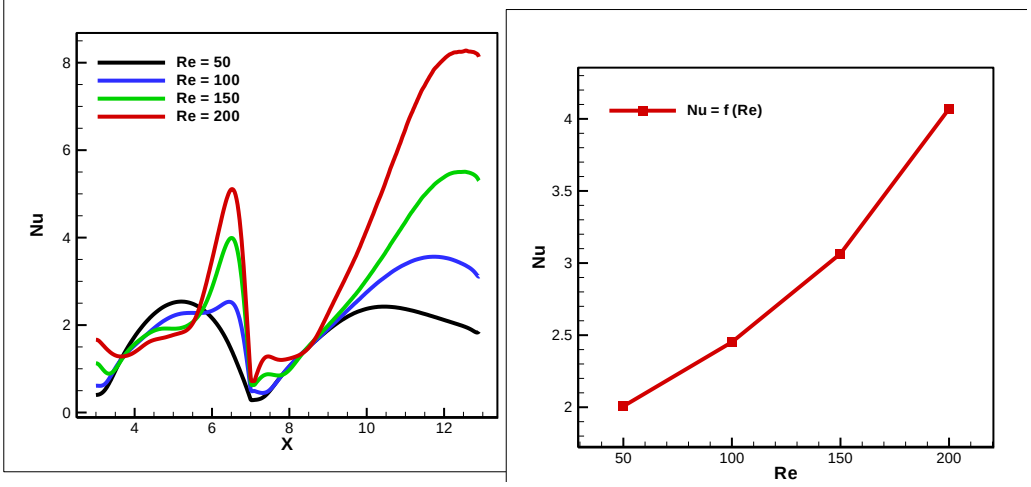

(a) Local Nusselt number (b) Average Nusselt number

Fig. 7: Local and average Nusselt number for different values of the Reynolds number

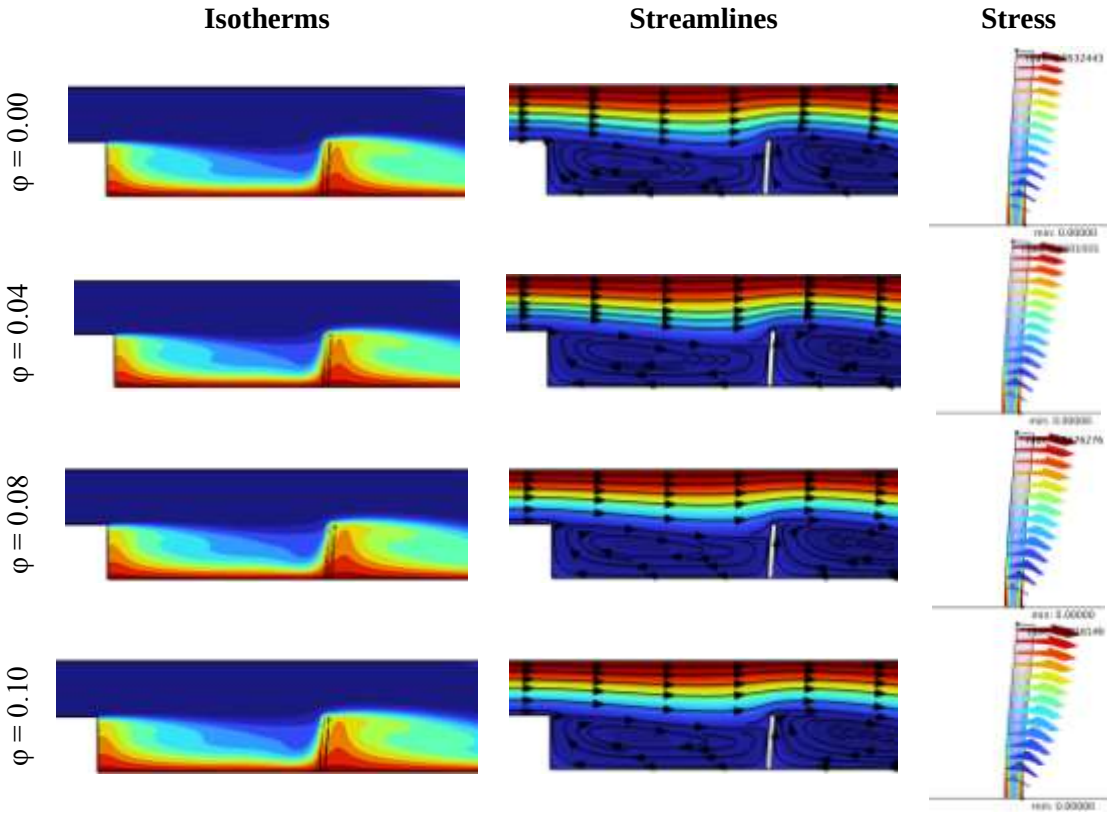

Fig. 8: Isotherms, streamlines, and stress for different nanoparticles volume fractions

4.2 Effect of the Volume Fraction

One of the main objectives of the present study is to highlight the influence of the volume fraction of CuO nanoparticles suspended in pure water on the thermal and hydrodynamic behavior of the nanofluid in the extended pipe and the thermal and mechanical behavior of the elastic structure. In this section, we analyze the impact of the addition of CuO nanoparticles on the mentioned behaviors.

Figure 8 shows the temperature and stream function contours, as well as the stress profile applied on the elastic fin, for different values of

volume fraction of CuO nanoparticles. The isotherms and stream function lines appear almost identical for the different considered volume fractions of nanoparticles, including pure water, except for a certain relative increase in the thickness of the thermal boundary layer and a certain decrease in the flow velocity. Due to the increase in pressure of the nanofluid as well as its viscous drag, the force imposed on the walls of the elastic structure increases relatively compared to the case of pure water flow.

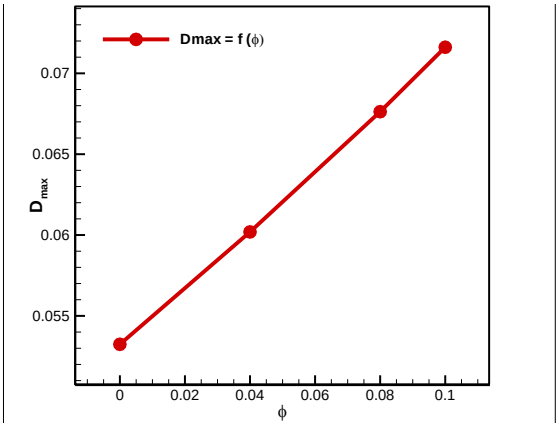

Fig 9. Maximal fin displacement for various nanoparticles volume fraction

This leads to an increase of the stress and consequently, it leads to a higher bending. Moreover, the maximum dimensionless displacement of the fin in the case of pure water flow is 0.053, however, for a nanofluid with a nanoparticle volume fraction of 0.1 the maximum displacement reaches 0.071, which presents a percentage of 34.58% compared to pure water. This is almost close to the percentage increase in viscosity of the nanofluid with 10% CuO concentration, as evident in Figure 9.

Regarding the heat transfer rate, it is recognized in the literature that the addition of nanoparticles to the base fluid improves this rate. Figure 10(a) shows that the local Nusselt number increases significantly with the increase of the volume fraction of CuO nanoparticles, especially downstream far from the structure and in the immediate upstream proximity of the fin. This situation informs about the development of the hydrodynamic state as a function of the volume fraction of CuO nanoparticles.

Indeed, far from the vortex zones where the fluid velocity is important, the convection rate grows and the impact of the nanoparticles on the heat transfer is more significant. On the other hand, due to the flexibility of the fin because of the nanoparticles, the flow becomes relatively fluid immediately upstream of the elastic structure so the rate of heat transfer is more notable. The average heat transfer enhancement rate along the hot wall as a function of the addition of CuO nanoparticles reaches 21.33% compared to the use of pure water, as shown in Figure 10 (b).

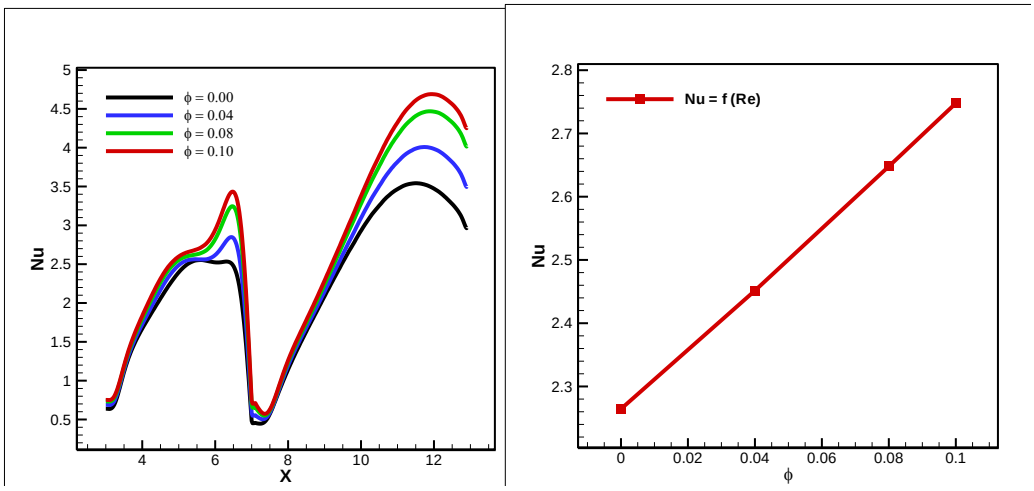

(a) Local Nusselt number (b) Average Nusselt number

Fig. 10: Local and average Nusselt number for various nanoparticles volume fraction

4.3 Effect of the Magnetic Field

Let us now focus on the influence of the density of a magnetic flux applied horizontally on the behavior of the nanofluid and the elastic fin. In this case, the Hartmann number is the dimensionless parameter to visualize the effect of the Lorentz force.

Figure 11 shows the isotherms, current lines, and the applied stress and fin displacement field for different values of the Hartmann number. At this angle of magnetic field application, the flow intensity inside the pipe decreases due to the perpendicular direction of the Lorentz electromagnetic force to the direction of flow.

Moreover, due to the decrease of the velocity as the Hartmann number increases, the two attachment vortices become almost dead zones where the fluid mobility is almost totally lost. On the other hand, the thickness of the thermal boundary layer increases with increasing values of Ha, indicating the predominance of the conductive heat transfer mechanism throughout the pipe. However, the load applied on the walls of the elastic structure increases.

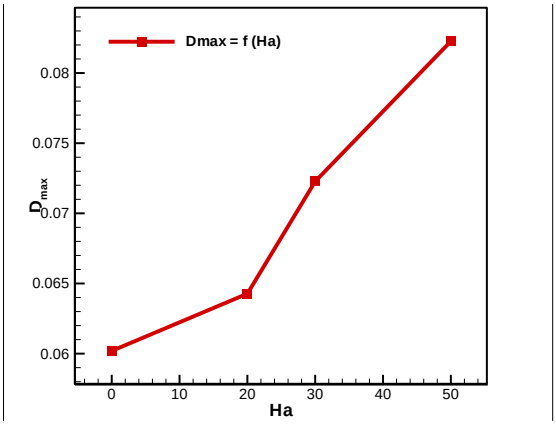

Fig. 12: Maximal fin displacement for various Hartmann numbers

The applied stress increases as the Hartmann number increases and the deformation becomes more significant. Indeed, at the upper interface of the structure, the pressure force applied on the fin walls is supported by the Lorentz force, leading to the increase of the displacement field intensity of the fin although the flow becomes very weak.

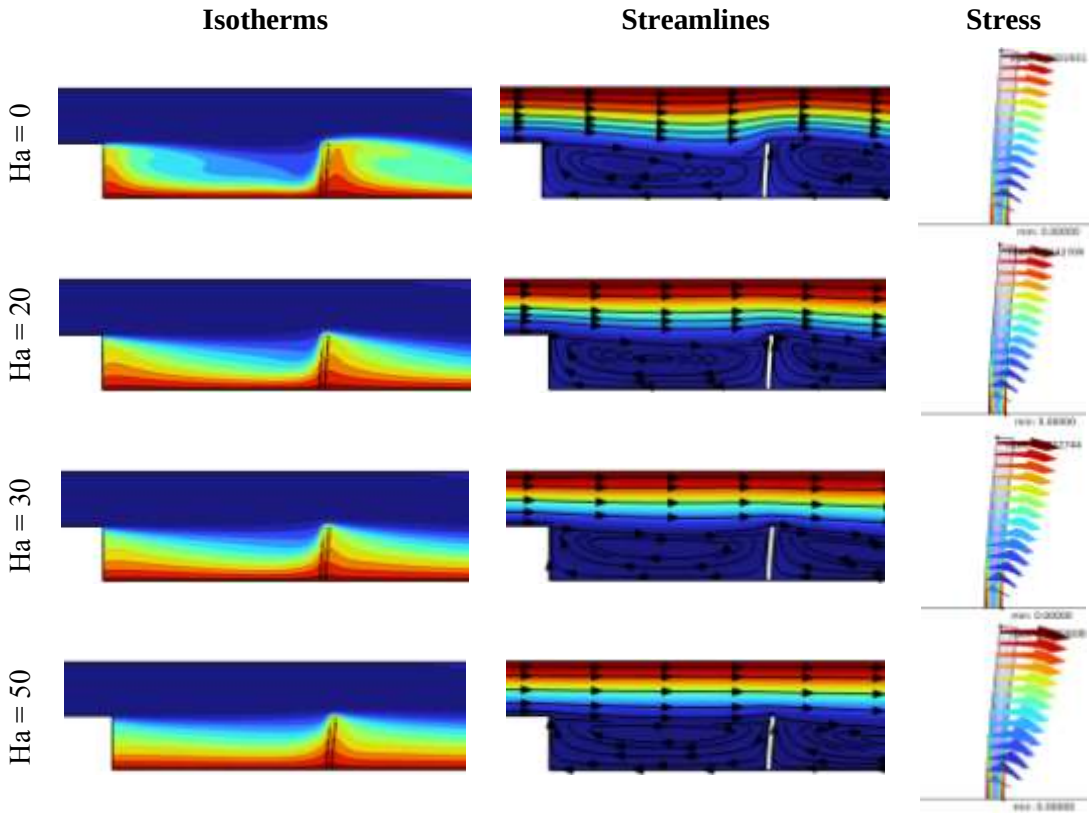

Fig. 11: Isotherms, streamlines, and stress for different Hartmann numbers

It should be noted that with a magnetohydrodynamic flow corresponding to a horizontal magnetic field intensity corresponding to Ha = 50, a maximum displacement percentage of 36.77% compared to a pure hydrodynamic flow arises, as shown in Figure 12.

Figure 13(a) shows the local Nusselt number along the hot wall of the pipe for different values of the Hartmann number. As already noticed, the heat transfer rate decreases significantly with increasing values of Ha, especially in the immediate downstream and upstream proximity of the elastic structure. However, at the level of the embedding zone, the rate of heat transfer appears almost identical whatever the value of Ha. Overall, the average heat transfer rate decreases significantly with the increase of the magnetic flux density, displaying a percentage decrease of almost 52% compared to the case of magnetic field absence, as shown in Figure 13(b).

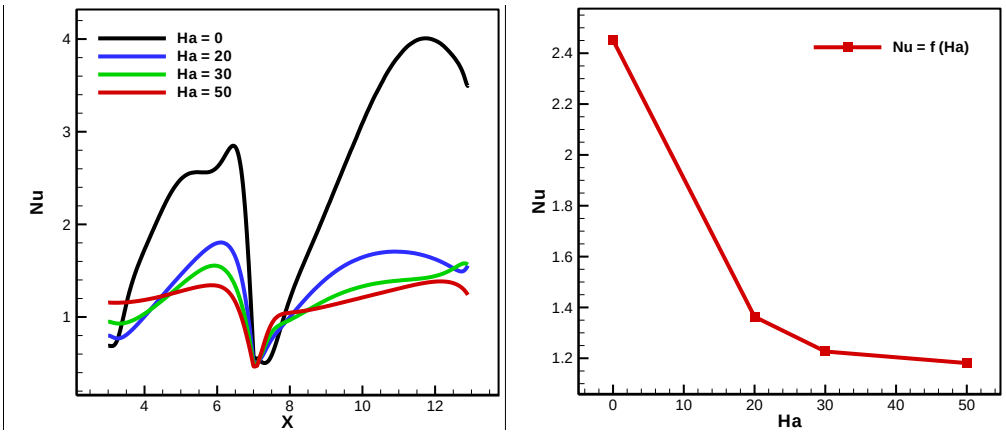

(a) Local Nusselt number (b) Average Nusselt number

Fig. 13: Local and average Nusselt numbers for various Hartmann numbers

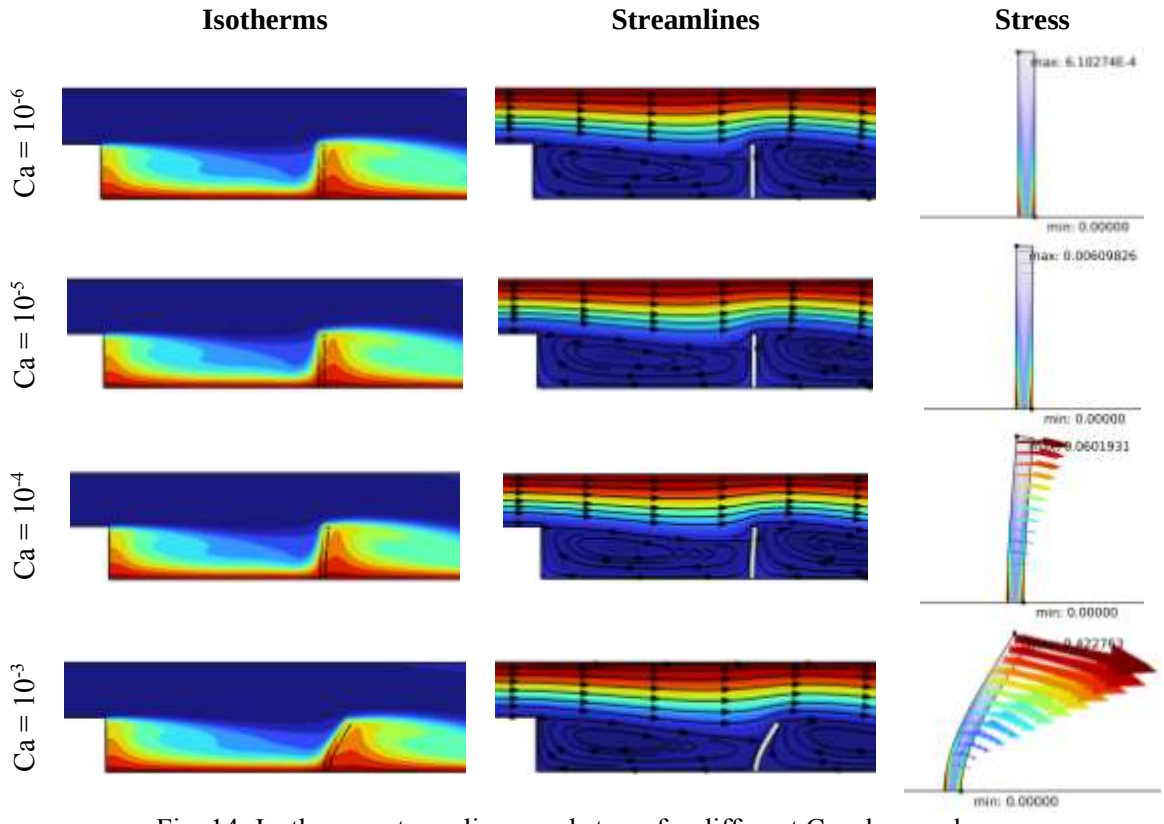

Fig. 14: Isotherms, streamlines, and stress for different Cauchy numbers

4.4 Effect of the Modulus of Elasticity

The modulus of elasticity presents an intrinsic quantity of the structure. In the present study, it translates the ability of the structure to resist before the load that it undergoes by the pressure force of the nanofluid as well as its viscous drag. The Cauchy number is a dimensionless parameter defined by the ratio between the reference pressure of the base fluid (ρu^2) and the elastic modulus (E). To this purpose, the increase in the Ca indicates that the modulus of elasticity decreases and therefore the solid structure becomes more and more elastic.

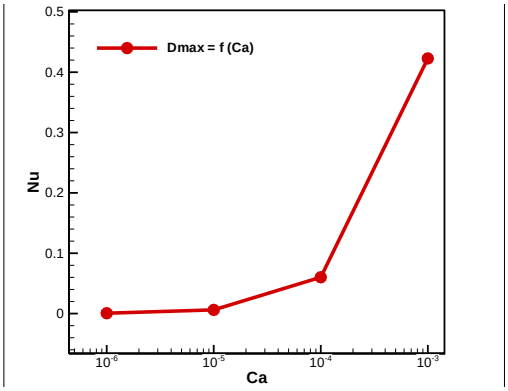

Fig. 15: Maximal fin displacement for various Cauchy number values.

Figure 14 shows the isotherms, the nanofluid streamlines, and the applied stress and displacement field of the elastic structure for different values of the Cauchy number. For Ca = 10^{-6}, the structure behaves as a non-deformable and rigid solid where the flow is completely blocked between the broadening region and the structure. However, with increasing values of the Cauchy number, the flexibility of the fin becomes more and more visible and very important for a Ca = 10^{-3}, where a maximum dimensionless displacement of 0.42 has been. Compared to the standard case of the study where Ca = 10^{-4}, a maximum dimensionless displacement of 0.06 is noted: this means that in the case Ca = 10^{-3} the displacement of the fin is six times greater than in the standard case, as shown in Figure 15.

Regarding the hydrodynamic and thermal structures of the nanofluid, with the increase of the Cauchy number from 10^{-6} to 10^{-4}, they are almost identical. In the case of a structure with a low modulus of elasticity, i.e. Ca = 10^{-3}, the flow becomes more fluid. Moreover, Figure 14 shows that the minimum intensity of the flow decreases. This is due to the enlargement of the vortex zone located upstream of the structure as well as to the possible formation of a weak secondary recirculation loop immediately downstream of the elastic structure.

Figure 16(a) presents the variation of the local Nusselt number along the hot wall for different values of the Cauchy number.

The figure shows that the heat transfer rate along this line remains almost identical for Cauchy numbers lower or equal to 10^{-4}, while for Ca=10^{-3} the heat transfer rate increases remarkably in the immediate proximity of the elastic fin. On the other hand, it decreases relatively beyond these areas exceptionally in the upstream part, due to the increase in the length of the vortex located in this area.

Regarding the average Nusselt number as a function of the Cauchy number, the overall heat transfer rate decreases slightly with the decrease of the modulus of elasticity, and after a certain threshold, it starts to increase relatively, due to the improvement of the heat transfer in the immediate proximity, as evident in Figure 16(b).

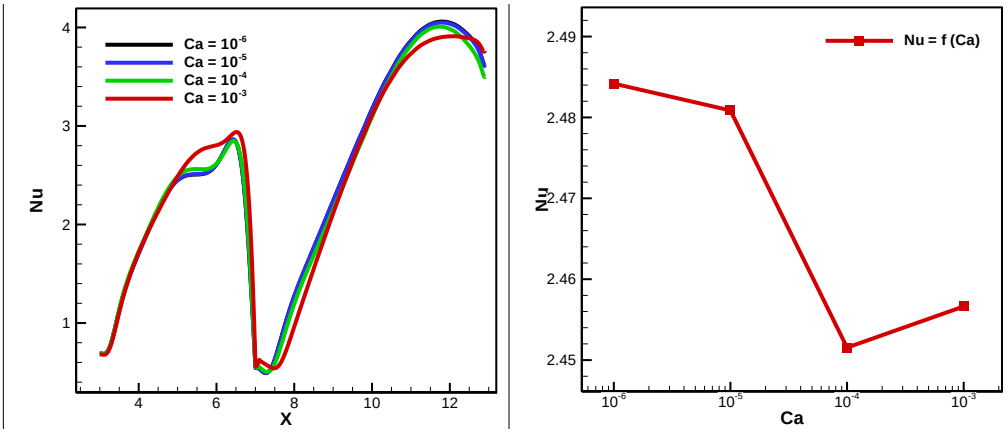

(a) Local Nusselt number (b) Average Nusselt number

Fig. 16: Local and average Nusselt numbers for various Cauchy numbers

5 Conclusion

In the present paper, a numerical investigation of the hydrodynamic and thermal behavior of the CuO-water nanofluid is presented. The geometry is a channel with an abruptly enlarged cross-section, and we focus on the elastic and thermal behavior of a solid fin (structure) installed inside the channel. Attention is paid to the influences of the flow velocity, the magnetic field, the concentration of nanoparticles as well as the elastic modulus of the structure on the thermal and mechanical behavior of the system. The main points obtained from this study are summarized as follows:

- The increase of the Reynolds number leads to the formation and intensification of two vortices. The first vortex is due to the enlargement of the section and the other is due to the presence of the fin at the bottom wall.
- The maximum fin displacement occurring at the upper corner of the fin decreases as Re increases since a large load downstream of the vane is applied in the opposite direction of flow as the Reynolds number increases.
- The heat transfer rate increases significantly with increasing values of Re, especially downstream of the elastic structure.
- The addition of CuO nanoparticles to pure water improves the local and global heat transfer rate by up to 21.33% compared to pure water. On the other hand, it causes an additional deformation of the elastic fin as well as an increase in internal stress due to the presence of the nanoparticles. This leads to the increase of its maximum displacement of 34.58% compared to the case of pure water flow.
- The application of a horizontal magnetic field to the CuO-water nanofluid flow significantly reduces the flow intensity within the pipe, especially in the vortex zones. Thus, the heat transfer rate is significantly reduced. Moreover, the Lorentz force applied vertically to the fin wall increases the deformation rate as well as the maximum displacement.
- The increase of the Cauchy number, inversely proportional to the modulus of elasticity, leads to an important flexibility of the fin and thus to its deformation. This leads to a relative reduction in terms of convective heat transfer rate, especially downstream of the fin, due to the widening of the vortex in this area and the creation of a weak secondary vortex below the bending zone.

Further developments of the present analysis will include an entropy generation analysis, and, more generally, experimental measures for a cross-validation of the results.

List of Symbols

B_0	Magnetic flux density
Ca	Cauchy number
Cp	Specific heat
E	Elasticity modulus
H	Channel Height
Ha	Hartmann number
k	Thermal conductivity
l	Fin thickness
N	Dimensionless normal coordinate
Nu	Nusselt number
p	Pressure
P	Dimensionless pressure
Pr	Prandtl number
Re	Reynolds number
T	Temperature
t	time
u	X-direction velocity
U	X-direction dimensionless velocity
u_0	Inlet velocity
u_s	X-direction fin (structure) velocity
v	Y-direction velocity
V	Y-direction dimensionless velocity
v_s	X-direction fin (structure) velocity
w	Fin displacement
W	Fin dimensionless displacement
x	Horizontal coordinate
X	Horizontal dimensionless coordinate
y	Vertical coordinate
Y	Vertical dimensionless coordinate

Greek symbols

α	Thermal diffusivity
γ	Magnetic field angle
θ	Dimensionless temperature
μ	Dynamic viscosity
ν	Cinematic viscosity
ρ	Density
σ	Electric conductivity
$\boldsymbol{\sigma}$	Stress tensor
τ	Dimensionless time
φ	Volume fraction
ψ	Stream function

Subscripts

p	Nanoparticles
f	Base fluid
nf	Nanofluid
0	Initial
max	Maximal value
s	Structure (solid)
r	Reference parameter.

References:

[1] Génevaux, O., Habibi, A., Dischler, J. M. (2003). Simulating Fluid-Solid Interaction. In Graphics Interface, Vol. 2003, pp. 31-38.

[2] Puliti, G., Paolucci, S., Sen, M., Nanofluids and their properties. *Applied Mechanics Reviews*, 64, 2011, 030383.

[3] Wang, X.Q., Mujumdar, A.S., A review on nanofluids-part I: theoretical and numerical investigations. *Brazilian Journal of Chemical Engineering*, 25, 2008, pp. 613-630.

[4] Selimefendigil, F., Öztop, H.F., Fluid-solid interaction of elastic-step type corrugation effects on the mixed convection of nanofluid in a vented cavity with magnetic field. *International Journal of Mechanical Sciences*, 152, 2019, pp. 185-197.

[5] Mehryan, S., Chamkha, A., Ismael, M., Ghalambaz, M., Fluid–structure interaction analysis of free convection in an inclined square cavity partitioned by a flexible impermeable membrane with sinusoidal temperature heating. *Meccanica*, 52, 2017, pp. 2685-2703.

[6] Ghalambaz, M., Jamesahar, E., Ismael, M.A., Chamkha, A.J., Fluid-structure interaction study of natural convection heat transfer over a flexible oscillating fin in a square cavity, *International Journal of Thermal Sciences*, 111, 2917, pp. 256-273.

[7] Shahabadi, M., Mehryan, S.A.M., Ghalambaz, M., Ismael, M., Controlling the natural convection of a non-Newtonian fluid using a flexible fin, *Applied Mathematical Modeling*, 92, 2020, pp. 669-686.

[8] Sabbar, W.A., Ismael, M.A., Almudhaffar, M., Fluid-structure interaction of mixed convection in a cavity-channel assembly of flexible wall. *International Journal of Mechanical Sciences*, 149, 2018, pp. 73-83.

[9] Rao, K.S., Sravani, K.G., Yugandhar, G., Rao, G.V., Mani, V.N., Design and analysis of fluid structure interaction in a horizontal micro channel. *Procedia Materials Science*, 10, 2020, pp. 768-788.

[10] Rossi di Schio, E., Impiombato, A.N., Mokhefi, A., Biserni, C., Theoretical and Numerical Study on Buongiorno's Model with a Couette Flow of a Nanofluid in a Channel with an Embedded Cavity, *Applied Sciences*, 12, 2022, 7751.

[11] Mokhefi, A., Rossi di Schio, E., Effect of a magnetic field on the Couette forced convection of a Buongiorno's nanofluid over an embedded cavity. *JP Journal of Heat and Mass Transfer* 30, 2022, pp. 89-104.

[12] Buongiorno, J., Convective Transport in Nanofluids. *ASME Journal of Heat Transfer*, 128, 2006, pp. 240–250.

[13] Rossi di Schio, E., Celli, M., Barletta, A., Effects of Brownian diffusion and thermophoresis on the laminar forced convection of a nanofluid in a channel. *ASME Journal of heat transfer*, 136(2), 2014, 022401.

[14] Sheikholeslami, M., Bhatti, M.M., Forced convection of nanofluid in presence of constant magnetic field considering shape effects of nanoparticles. *International Journal of Heat and Mass Transfer*, 111, 2017, pp. 1039-1049.

[15] Sheikholeslami, M., Magnetohydrodynamic nanofluid forced convection in a porous lid driven cubic cavity using Lattice Boltzmann method. *Journal of Molecular Liquids*, 231, 2017, pp. 555-565.

[16] Jamesahar, E., Sabour, M., Shahabadi, M., Mehryan, S. A. M., Ghalambaz, M., Mixed convection heat transfer by nanofluids in a cavity with two oscillating flexible fins: A fluid–structure interaction approach. *Applied Mathematical Modelling*, 82, 2020, pp. 72-90.

[17] Selimefendigil, F., Öztop, H.F., Forced convection in a branching channel with partly elastic walls and inner L-shaped conductive obstacle under the influence of magnetic field. *International Journal of Heat and Mass Transfer*, 144, 2019, 118598.

[18] Sotiropoulos, F., Yang, X., Immersed boundary methods for simulating fluid–structure interaction. *Progress in Aerospace Sciences*, 65, 2014, pp. 1-21.

[19] Mehryan, S-.A.M., Ghalambaz, M., Ismael, M.A., Chamkha, A.J., Analysis of fluid-solid interaction in mhd natural convection in a square cavity equally partitioned by a vertical flexible membrane, *Journal of Magnetism and Magnetic Materials* 424, 2017, pp. 161-173.

[20] Hussain S, Ahmed SE, Akbar T., Entropy generation analysis in MHD mixed convection of hybrid nanofluid in an open cavity with a hori-zontal channel containing an adiabatic obstacle. *International Journal of Heat and Mass Transfer*, 114, 2017, pp. 1054–1066.

Contribution of Individual Authors to the Creation of a Scientific Article (Ghostwriting Policy)

The authors equally contributed to the present research, at all stages from the formulation of the problem to the final findings and solution.

Sources of Funding for Research Presented in a Scientific Article or Scientific Article Itself

No funding was received for conducting this study.

Conflict of Interest

The authors have no conflicts of interest to declare that are relevant to the content of this article.